1 # Lipogenesis and innate immunity in hepatocellular
2 # carcinoma cells reprogrammed by an isoenzyme switch of
3 # hexokinases

4 **Laure Perrin-Cocon[1],†, Pierre-Olivier Vidalain[1],†, Clémence Jacquemin[1], Anne Aublin-Gex[1],**
5 **Keedrian Olmstead[2], Baptiste Panthu[1,3], Gilles J. P. Rautureau[4], Patrice André[1], Piotr Nyczka[5],**
6 **Marc-Thorsten Hütt[5], Nivea Amoedo[6], Rodrigue Rossignol[6,7], Fabian Volker Filipp[2,8], Vincent**
7 **Lotteau[1],*‡ Olivier Diaz[1],*‡**

8 1- CIRI, Centre International de Recherche en Infectiologie, Univ Lyon, Inserm, U1111, Université
9 Claude Bernard Lyon 1, CNRS, UMR5308, ENS de Lyon, 21 Avenue Tony Garnier, F-69007, Lyon,
10 France.
11 2- Cancer Systems Biology, Institute of Computational Biology, Helmholtz Zentrum München,
12 Ingolstädter Landstraße 1, D-85764, München, Germany.
13 3- Actual address: Univ Lyon, CarMeN Laboratory, Inserm, INRA, INSA Lyon, Université Claude
14 Bernard Lyon 1, F-69921, Oullins Cedex, France.
15 4- Université de Lyon, CNRS, Université Claude Bernard Lyon 1, ENS de Lyon, Centre de RMN à
16 Très Hauts Champs (CRMN), FRE 2034, F-69100 Villeurbanne, France.
17 5- Department of Life Sciences and Chemistry, Jacobs University, Bremen, Germany.
18 6- CELLOMET, Centre de Génomique Fonctionnelle de Bordeaux, 146 Rue Léo Saignat, F-33000
19 Bordeaux, France.
20 7- Univ. Bordeaux, Inserm, MRGM, U1211, F-33076, Bordeaux, France.
21 8- School of Life Sciences Weihenstephan, Technical University München, Maximus-von-Imhof-
22 Forum 3, D-85354, Freising, Germany.
23
24 † These authors contributed equally to this work
25 ‡These authors jointly supervised this work
26
27 *** Corresponding authors:**
28 vincent.lotteau@inserm.fr (ORCID: 0000-0003-0997-3282)
29 olivier.diaz@inserm.fr (ORCID: 0000-0002-3451-9914)
30
31
32
33
34
35 **Keywords**
36 Hepatocellular carcinoma, hexokinase, lipogenesis, innate immunity, lipoproteins.
37
38
39
40 **This PDF file includes:**
41 Main Text
42 Figures 1 to 7
43

44

Abstract

During the cancerous transformation of normal hepatocytes into hepatocellular carcinoma (HCC), the enzyme catalyzing the first rate-limiting step of glycolysis, namely the glucokinase (GCK), is replaced by the higher affinity isoenzyme, hexokinase 2 (HK2). The transcriptomic analysis of HCC tumors shows that highest expression level of *HK2* in tumor lesions is inversely correlated to *GCK* expression, and is associated to poor prognosis for patient survival. To further explore functional consequences of the GCK-to-HK2 isoenzyme switch occurring during carcinogenesis, *HK2* was knocked-out in the HCC cell line Huh7 and replaced by *GCK*, to generate the Huh7-*GCK$^+$/HK2$^-$* cell line. HK2 knockdown and GCK expression rewired central carbon metabolism, stimulated mitochondrial respiration and restored essential metabolic functions of normal hepatocytes such as lipogenesis, VLDL secretion, glycogen storage. It also reactivated innate immune responses and sensitivity to natural killer cells, showing that consequences of the HK switch extend beyond metabolic reprogramming.

Main Text

Introduction

Hepatocellular carcinoma (HCC) is the most common liver cancer and the fourth leading cause of cancer-related death (1). HCC is closely linked to chronic liver inflammation, chronic viral hepatitis, exposure to toxins, and metabolic dysfunction such as non-alcoholic steatohepatitis (NASH). HCC is of poor prognosis, and treatments are essentially based on surgical resection, liver transplantation or aggressive chemo and/or radiotherapy. In patients with advanced HCC, broad-spectrum kinase inhibitors are approved (2) but with limited benefit (3). Effective personalized therapies are needed but their development is impeded by our poor understanding of molecular mechanisms underlying HCC onset and progression. Efforts to characterize the disease on the

2

71   basis of etiology and outcomes revealed metabolic deregulation as a hallmark of HCC progression

72   (4). Indeed, metabolic remodeling is critically required for tumor growth, since bioenergetic

73   requirements and anabolic demands drastically increase (5–7). For instance, HCC cells have lost

74   their ability to secrete very low-density lipoproteins (VLDL), a highly specialized function of

75   hepatocyte and can only secrete low-density lipoproteins (LDL)-like lipoproteins, indicating a

76   defective lipogenesis and/or lipoprotein assembly (8).

77   Metabolic reprogramming in cancer cells involves the modulation of several enzymes by

78   oncogenic drivers (6). Targeting these enzymes is now considered as a therapeutic strategy for

79   several types of cancers (6). Among these enzymes, hexokinase 2 (HK2) stands out because of its

80   elevated or induced expression in numerous cancers, including HCC (9). Hexokinases control the

81   first rate-limiting step of glucose catabolism by phosphorylating glucose to glucose-6-phosphate

82   (G6P), fueling glycolysis as well as glycogen, pentose phosphate and triglyceride synthesis. The

83   human genome contains four genes encoding distinct hexokinase isoenzymes, named HK1 to HK4

84   (HK4 is also known as glucokinase or GCK), with distinct enzymatic kinetics and tissue

85   distributions. A fifth putative hexokinase enzyme was recently discovered but has not been fully

86   characterized yet (10). A switch from GCK to HK2 isoenzymes is occurring during the transition

87   from primary to tumor hepatocytes so that HCC cell lines express HK2 but no longer GCK. HK2

88   expression level has been correlated with disease progression and dedifferentiation of HCC cells

89   (11). When HK2 is artificially knocked-down in HCC cell lines, glycolysis is repressed, and

90   tumorigenesis is inhibited while cell death increases (9). In addition, hexokinase function extends

91   beyond metabolism towards autophagy, cell migration, and immunity, suggesting that the GCK-

92   to-HK2 isoenzyme switch has broader consequences than initially suspected (12–15). Here, we

93   analyzed transcriptomic data of HCC biopsies and correlated hexokinase isoenzyme expression

94   level with patient survival. This led us to generate a new human HCC model expressing *GCK*

95   instead of *HK2*. A comparative analysis of *GCK⁺ vs HK2⁺* HCC cell lines provided a unique

96   opportunity to look into HK isoenzyme-dependent metabolic features, lipoprotein production and

97   resistance to immune signals of liver cancer cells.

Results

Relative expression level of GCK and HK2 in HCC patients

100   Although an isoenzyme switch from GCK to HK2 has been observed during the carcinogenesis

101   process (16), whether hexokinase isoenzymes expression is predictive of patient survival is

102   unclear. We first analyzed the transcriptomes (RNAseq data) of 365 HCC biopsies from The Cancer

103   Genome Atlas (TCGA) database (17, 18)(Supplementary Table 1). For each HK, the individual gene

104   expression level was used to stratify patients into two subgroups according to Uhlen et al. (18)

105   and overall survival in the two subgroups was determined using a Kaplan-Meier's estimator.

106   Although *HK1* or *HK3* expression level were not associated to patient survival rate (Fig. 1a), highest

107   expression levels of *HK2* as previously described (19) and lowest expression levels of *GCK* in the

108   tumors were associated with a lower survival rate. We thus stratified patients based on the

109   GCK/HK2 expression ratio to combine these two markers (Fig. 1b). When patients were stratified

110   on the basis of *HK2* or *GCK* expression levels, the median survival between the corresponding

111   subgroups differed by 33.8 and 36.5 months, respectively (Fig. 1a). This difference reached 42.8

112   months when the stratification of patients was based on the *GCK/HK2* ratio (Fig. 1b). This

113   demonstrated that the *GCK/HK2* ratio outperforms *HK2* or *GCK* expression alone as predictor of

114   patient survival. Finally, correlation coefficients between patient survival in months and *HK2* or

115   *GCK* expression level were determined. For this, we only considered the subset of 130 patients

116   for whom the period between diagnosis and death is precisely known (uncensored data), and

4

117   performed a Spearman's rank correlation test (Fig. 1c). Patient survival was positively correlated

118   to *GCK* expression but inversely correlated to *HK2* expression in line with the Kaplan-Meier

119   analysis. In addition, *GCK* and *HK2* expression tends to be inversely correlated in tumor samples

120   (Fig. 1c). Therefore, there is a trend for mutual exclusion of *GCK* and *HK2* expression in HCC

121   tumors, and this profile is associated to clinical outcome.

122   **Engineering a cellular model of the hexokinase isoenzyme switch**

123   To decipher functional consequences of GCK or HK2 expression in a HCC model, we restored GCK

124   expression by lentiviral transduction in the reference HCC cell line Huh7, and knocked-out the

125   endogenous *HK2* gene by CRISPR/Cas9. The exclusive expression of HK2 and *GCK* in Huh7 and

126   Huh7-*GCK$^+$/HK2$^-$* cell lines, respectively, was validated, while HK1 and HK3 were not expressed

127   (Fig. 2a). The hexokinase activity in the presence of increasing concentration of glucose was

128   determined in protein lysates from the two respective cell lines. Hexokinase activity in Huh7 lysate

129   reached its maximum at low glucose concentration, presenting a saturation curve according to

130   Michaelis–Menten kinetics (Fig. 2b). In contrast, the hexokinase activity in Huh7-*GCK$^+$/HK2$^-$*

131   lysates followed a pseudo-allosteric response to glucose (20, 21). Thus, the expected HK2 and GCK

132   activities were observed in the Huh7 and Huh7-*GCK$^+$/HK2$^-$* cells respectively. The cell proliferation

133   capacity remained identical between the two cell lines (Supplementary Fig. 1). We then compared

134   the genome edited Huh7-*GCK$^+$/HK2$^-$* and the parental Huh7 cell lines (*i.e.* Huh7-*GCK$^-$/HK2$^+$*) at a

135   transcriptomic, metabolic and immunological level.

136   **Transcriptomic data revealed extended modifications of metabolic connections in Huh7-**

137   **GCK+/HK2-**

138   Transcriptomic profiles of Huh7 and Huh7-*GCK$^+$/HK2$^-$* cells were determined by next generation

139   sequencing (Supplementary Table 2). Overall, 4.2% of the gene transcripts were reduced and 6.9%

140 were induced in Huh7-$GCK^+/HK2^-$ compared to Huh7 (Fig. 2c; |fold-change (FC)|>2 and p

141 value<0.05). We first determined the metabolic consequences of the HK isoenzyme switch by

142 mapping the differentially expressed genes onto the a well-established bipartite metabolic

143 network Recon2, connecting gene products and metabolites (Supplementary Fig. 2-4) (22, 23).

144 After trimming highest-degree metabolites as currency metabolites, clusters of genes that are

145 both differentially expressed and connected by common metabolites emerged. Interestingly, we

146 found that across a wide range of analysis parameters, including varying rates of currency

147 metabolites and gene expression fold-change, the differentially expressed metabolic genes are

148 substantially better connected than expected by chance (Fig. 2d). This highlights the specificity of

149 the transcriptomic changes with respect to metabolic pathways. The spanned network presented

150 in Figure 2e corresponds to a stringent fold-change threshold for transcriptomic data

151 ($\log_2(|FC|)>3$) while removing 2 percent of highest-degree currency metabolites. This network

152 shows connected components within glycolysis, but also across distant modules including the

153 gamma-aminobutyric acid (GABA) shunt (ALDH5A1), urea cycle (CPS1, OTC), glycogen metabolism

154 (GYS1, GYS2, AGL) and lipid synthesis (GPAM, AGPAT4, DGKG, CDS1, A4GALT) or degradation

155 (ACADL, HSD17B4, AMACR). This analysis highlights the global impact of the HK isoenzyme switch

156 that spreads beyond glycolysis across distant connected metabolic modules.

157 Enrichment of molecular and cellular functions in differentially expressed genes was also analyzed

158 using Ingenuity Pathway Analysis (IPA). This revealed that cellular movement and lipid

159 metabolism were the most affected functions (Fig. 3a and Supplementary Table 3). A closer look

160 at these annotations pointed to differences in the migratory capacities (Fig. 3b) as well as lipid

161 concentration and synthesis (Fig. 3c). The migratory capacities of Huh7 and Huh7-$GCK^+/HK2^-$ were

162 compared using transwell-migration cell assays (Fig. 3d-e). Results showed a higher migratory

163   capacity of Huh7-*GCK+/HK2-* cells, in line with Kishore M. et al showing that GCK expression

164   induced by pro-migratory signals controls the trafficking of CD4+/CD25+/FOXP3+ regulatory T (T$_{reg}$)

165   cells (15). To validate the differences in lipid metabolism highlighted by the transcriptomic

166   analysis, intracellular content in neutral lipids was first determined with lipophilic dyes. As

167   assessed by Oil-Red-O or BODIPY staining, an accumulation of intracellular neutral lipids was

168   observed in Huh7-*GCK+/HK2-* in comparison to Huh7 (Fig. 3f and 3g). The accumulation of neutral

169   lipids in Huh7 expressing both *HK2* and *GCK* indicates that the phenotype is driven by *GCK*

170   expression and not by *HK2* knockdown (Supplementary Fig. 5). Lipid accumulation upon GCK

171   expression was also observed in Huh6 hepatoblastoma cells but not in epithelial kidney Vero cells,

172   indicating that this phenomenon occurs in metabolically relevant cells (Supplementary Fig. 5).

173   **Differential lipid metabolism in Huh7 and Huh7-*GCK+/HK2-***

174   The intracellular lipid content of the two cell lines was further analyzed. In Huh7-*GCK+/HK2-*, an

175   enrichment in phosphatidylcholine, cholesterol, triglycerides (TG) and free fatty acids was

176   observed compared to Huh7 (Fig. 4a). One major function of hepatocytes is to secrete triglyceride-

177   rich VLDL and this function is altered in HCC cells that secrete smaller lipoproteins with the density

178   of LDL (24, 25). The secretion of lipids and lipoproteins by both cell lines was analyzed after a 24h-

179   culture in the absence of FCS to exclude any participation of exogenous lipids in the production

180   of lipoproteins. Huh7-*GCK+/HK2-* secreted more free fatty acids than Huh7 while secretion of

181   cholesterol and triglycerides (TG) remained unchanged (Fig. 4b). However, under the same

182   conditions, the secretion of apolipoprotein B (ApoB) by Huh7-*GCK+/HK2-* was reduced compared

183   to Huh7. Since ApoB is a non-exchangeable protein with only one copy in VLDL and LDL particles,

184   an elevated TG/ApoB ratio indicates that ApoB+-lipoproteins secreted by Huh7-*GCK+/HK2-* cells

185   are enriched in TG compared to those secreted by Huh7 (Fig. 4c). This was confirmed by the ApoB

186   distribution in density gradient fractions. As expected, lipoproteins secreted by Huh7 sediment at

187   the density of LDL, while those secreted by Huh7-*GCK+/HK2-* (Fig. 4d) match the density of VLDL

188   found in human plasma or secreted by primary human hepatocytes in culture (26, 27). This

189   indicates that GCK expression is essential for the VLDL assembly/secretion pathway and could

190   explain the loss of this crucial metabolic pathway in hepatoma cells expressing HK2 instead of GCK

191   (28).

192   **Differential activity of the tricarboxylic acid cycle (TCA) in Huh7 and Huh7-*GCK+/HK2-***

193   We observed that GCK expression increased the intracellular content in lipids, resulting in

194   accumulation of lipid droplets and secretion of VLDL. A rewiring of cellular metabolism towards

195   energy storage in Huh7-*GCK+/HK2-* was thus suspected and confirmed by the accumulation of

196   glycogen, creatinine and creatinine-P (Fig. 5a and b), a feature of functional hepatocytes. To

197   further determine the consequences of replacing HK2 by GCK, we quantified prominent

198   intracellular metabolites via GC-MS. Figure 5c shows relative intracellular quantities of

199   metabolites that are significantly different between Huh7 and Huh7-*GCK+/HK2-*. Among

200   differentially represented metabolites, higher levels of glucose, glycerol-3-phosphate and lactic

201   acid were detected in Huh7-*GCK+/HK2- cells*. Several intermediates of the TCA cycle (succinic acid,

202   fumaric acid, alpha-ketoglutaric acid), and metabolites directly connected to it (GABA, glutamic

203   acid, glutamine, aspartic acid) were also differentially present between the two cell lines. This

204   supports a significant modulation of central carbon metabolism at both the level of glycolysis and

205   TCA cycle. This led to investigate glucose catabolism in further details. Glucose consumption and

206   stable isotope incorporation from [U-^{13}C]-glucose into pyruvate were both increased in Huh7-

207   *GCK+/HK2-*cells compared to Huh7 cells (Fig. 5d and f). This increased glycolytic flux together with

208   a reduced lactate secretion (Fig. 5e) is likely to account for the elevation of lactate levels and

8

209   suggest that the increased pyruvate production essentially fuels mitochondrial TCA cycle in Huh7-

210    $GCK^+/HK2^-$ cells.

211   Pyruvate entering the mitochondria downstream of glycolysis can be either oxidized by pyruvate

212   dehydrogenase (PDH), producing acetyl-CoA, or converted into oxaloacetate (OAA) by pyruvate

213   carboxylase (PC). Acetyl-CoA and OAA are then combined in the TCA cycle to form citrate. *De novo*

214   lipogenesis requires citrate egress from the TCA cycle to serve as a precursor of cytosolic acetyl-

215   CoA for further synthesis of fatty acids. In Huh7-$GCK^+/HK2^-$ cells, we observed both an increased

216   activity of PC (Fig. 5g) without changes in protein expression (Fig. 5h) and an increased

217   phosphorylation of pyruvate dehydrogenase (PDH), which is indicative of a reduced activity of this

218   enzyme (Fig. 5i). This is consistent with the increased expression of the PDH kinase PDK2 and the

219   decreased expression of the PDH phosphatase PDP2 in Huh7-$GCK^+/HK2^-$ cells that regulate the

220   PDH phosphorylation state (Fig. 5j). A rebalanced usage of pyruvate in Huh7-$GCK^+/HK2^-$ cells

221   maintains a functional TCA cycle and supports lipogenesis. In Huh7-$GCK^+/HK2^-$ cells, we also

222   observed an increased phosphorylation of ATP citrate lyase (ACLY), the first enzyme of the fatty

223   acid synthesis pathway, indicating an enhanced activity of this enzyme (Fig. 5k). This reaction also

224   regenerates OAA in the cytosolic compartment. Interestingly, transcriptomic data show that PCK1

225   which converts OAA to phosphoenolpyruvate (PEP), is overexpressed in Huh7-$GCK^+/HK2^-$cells

226   compared to Huh7 (FC > 32).

227   A shift from pyruvate oxidation to carboxylation is observed in cancer cells where succinate

228   dehydrogenase (SDH) is inactivated by mutation and OAA can only be generated through PC

229   activity (29). SDH inhibition leads to succinate accumulation, especially in activated immune cells

230   (30). Interestingly, higher levels of succinate and a reduced activity of SDH were measured in

231   Huh7-$GCK^+/HK2^-$ cells compared to Huh7 (Fig. 5l and m). Even though SDH is also part of the

9

232 complex II of the mitochondrial respiratory chain, we observed that the overall oxygen

233 consumption was increased in Huh7-$GCK^+/HK2^-$ (Fig. 5n) with increased basal and maximal

234 respiration, ATP production and spare respiration capacity (Supplementary Fig. 6). Functional

235 analysis of the respiratory chain showed that oxygen consumption in Huh7 and Huh7-$GCK^+/HK2^-$

236 cells was mainly dependent on complex I which is fueling complex III (Fig. 5n and o). Thereby, the

237 HK isoenzyme switch rewired the TCA cycle promoting carboxylation of pyruvate into OAA in the

238 presence of a reduced SDH activity and increased respiration through complex I.

239 **Restored innate immune sensitivity in Huh7-$GCK^+/HK2^-$**

240 Lipid accumulation in hepatocytes is incriminated in hepatic inflammation (31) and TCA cycle

241 rewiring is associated with innate immunity activation (32). These two events were observed

242 when replacing HK2 by GCK in Huh7 cells, questioning the immune status of these cells and their

243 sensitivity to antitumor immunity. The functional analysis of gene ontology (GO) terms associated

244 to differentially expressed transcripts revealed an enrichment in terms related to the regulation

245 of innate immunity. The gene signature associated with type-I interferon (IFN) signaling pathway

246 scored among the top enriched terms of upregulated genes in Huh7-$GCK^+/HK2^-$ cells

247 (Supplementary Fig. 7). Within the 91 gene members of this GO term, 20 transcripts of Type I-IFN

248 signaling were significantly up-regulated in Huh7-$GCK^+/HK2^-$ compared to Huh7 (Fig. 6a). This

249 includes interferon regulatory factors (IRF1, IRF7 and IRF9), IFN-stimulated genes (ISGs) such as

250 ISG15, MX1, OAS1, OAS3, RNaseL and signaling intermediates such as IKBKE coding for IKKε (Fig.

251 6b). The chaperon HSP90AB1, which is involved in the phosphorylation and activation of STAT1,

252 was also induced (33). In contrast, two genes were significantly down-regulated in Huh7-

253 $GCK^+/HK2^-$ compared to Huh7, the RNaseL inhibitor ABCE1, and TRIM6, an E3 ubiquitin-protein

254 ligase regulating IKKε. Among the members of the RIG-I-like receptor (RLR) family involved in

10

255   immune sensing and antitumor defense (34), the expression of IFIH1 (also known as MDA5) was

256   slightly increased in Huh7-GCK^+/$HK2^-$, while RIG-l itself remained unchanged. Such identified gene

257   sets suggest that Huh7-GCK^+/$HK2^-$ cells may be better equipped than Huh7 cells to respond to

258   innate immune signals. Thus, we compared the innate immune response of the two cell lines

259   when stimulated by RIG-I or MDA5 ligands, known to sense different double-stranded RNA

260   (dsRNA) in viral immune recognition. In order to quantify cellular activation by dsRNA, immuno-

261   stimulatory challenge assays were conducted with triphosphate-hairpin RNA (3p-hpRNA) or

262   polyinosinic-polycytidylic acid (poly(I:C)). Interferon-sensitive response element (ISRE)-

263   dependent transcription was efficiently induced by these RLR ligands in Huh7-GCK^+/$HK2^-$ cells

264   whereas Huh7 response was very limited even at high doses of immuno-stimulatory ligands (Fig.

265   6c).

266   To investigate whether this differential sensitivity to RLR ligands is linked to GCK expression or

267   HK2 knockout, we used Huh7 cells transduced for GCK expression so that they express both HK2

268   and GCK (Huh7-GCK^+/$HK2^+$). In these cells, the response to RIG-I ligation did not differ from that

269   of Huh7 cells suggesting that GCK expression alone is not sufficient to restore immune sensitivity

270   (Fig. 6d). When HK2 expression was repressed in these cells with a shRNA (Huh7-GCK^+/$HK2^-$Sh)

271   (see Supplementary Fig. 8 showing 95% extinction of HK2 protein), ISRE response to RIG-I signaling

272   was restored to a level similar to that observed in Huh7-GCK^+/$HK2^-$ cells (Fig. 6d). This is pointing

273   towards HK2 as a negative regulator of RLR signaling in HCC cells and suggests that the *GCK*-to-

274   *HK2* isoenzyme switch during malignant transformation of hepatocytes is accompanied by a

275   reduced sensitivity to innate immune signals. The higher sensitivity to RLR ligands of Huh7-

276   GCK^+/$HK2^-$ cells also resulted in increased secretion of inflammatory interleukins (IL-6 and IL-8),

277   antiviral cytokines (IFN-λ_1, IFN-$\lambda_{2/3}$, IFN-β), and IP-10 (Fig. 6e), indicating that both NF-κB- and

278   IRF3-dependent signaling pathways were induced. IL-1β, TNFα, IL-12p70, GM-CSF, IL-10 and IFNγ

279   were not detected in the supernatants of none of the cell lines, whether they were stimulated or

280   not.

281   As natural killer (NK) cell-mediated lysis of tumor cells is crucial for the anti-cancer immune

282   defense, we compared the susceptibility of the two cell lines to NK cells cytotoxicity. Figure 6f

283   shows that Huh7 cells are resistant to NK cell-mediated lysis in contrast to Huh7-$GCK^+/HK2^-$. Thus,

284   replacing HK2 by GCK restored Huh7 sensitivity to NK cell-mediated lysis. Similar results were

285   obtained when NK cells were pre-activated with IL-2 (Supplementary Fig. 9). Altogether, these

286   results demonstrate that HCC cells expressing HK2 instead of GCK exhibit an impaired response

287   to immune signals and also a strong resistance to NK cells. Significantly, these two observations

288   are in line with clinical data showing that elevated GCK expression is associated with prolonged

289   survival, while elevated HK2 expression coinciding with GCK reduction correlates with shorter

290   overall survival (Fig. 1).

291   **Discussion**

292   Metabolic network rewiring is a hallmark of cancer although for most tumors, mechanisms at the

293   origin of this metabolic reprogramming have not been elucidated. While GCK, but not HK2, is

294   expressed in normal hepatocytes, the expression of HK2 occurs during cirrhosis and increases as

295   the disease progresses to carcinoma. Several signaling pathways such as hypoxia inducible factors

296   (HIF), peroxisome proliferator-activated receptors (PPAR) and phosphatidylinositol-4,5-

297   bisphosphate 3-kinase (PI3K) might contribute to HK2 induction in fatty liver disease and its

298   evolution towards cirrhosis and carcinogenesis (35–37). Consequently HK2 induction has been

299   proposed as a risk marker of HCC development (16). Analyzing TCGA data from human HCC

300   tumors, we observed that not only high levels of *HK2* but also low levels of *GCK* are of poor

301   prognosis. In contrast, neither *HK1* nor *HK3* expression levels were correlated with survival of HCC

302   patients. *GCK* expression is very low or not detected in biopsies from a majority of patients (65.8%

303   of patients show RSEM values <10), whereas *HK2* is widely expressed (16) (only 5.8% of patients

304   show RSEM values <10). This probably explains that HK2 expression is a better prognostic marker

305   than GCK for HCC. However, when GCK and HK2 expression were combined into a single ratio,

306   this prognostic marker outperformed HK2 or GCK expression alone. This suggests that both HK2

307   induction and GCK loss play a role in HCC progression. As HK2 and GCK expression tend to be

308   mutually exclusive, both HK2 induction and GCK downregulation might have consequences on the

309   metabolic reprogramming during malignant transformation of hepatocytes. To compare the

310   functional consequences of the HK isoenzyme switch in HCC, we therefore expressed GCK in the

311   reference HCC cell line Huh7 and knocked-down HK2 expression. Our comparative transcriptomic,

312   metabolic and functional studies demonstrate that the replacement of HK2 by GCK not only

313   restored some essential metabolic functions of normal hepatocytes such as lipogenesis, VLDL

314   secretion and glycogen storage but also reactivated innate immune responses and sensitivity to

315   NK-mediated cell lysis.

316   HCC cell lines predominantly secrete LDL-like particles, unlike normal hepatocytes, which secrete

317   VLDL. Lipid loading of Huh7 cells with oleic acid can boost the secretion of ApoB$^+$ particles but

318   does not induce a shift from LDL to VLDL density, indicating that intracellular fatty acid

319   accumulation of exogenous origin cannot rescue VLDL production (28). Here we show that

320   replacing HK2 by GCK in Huh7 cells restored *de novo* fatty acid synthesis, allowing VLDL

321   assembly/secretion in the absence of exogenous lipids. To our knowledge Huh7-*GCK$^+$/HK2$^-$* is the

322   first human cell model with a functional VLDL secretion pathway. Such a tool will strongly benefit

323   the field of cardiovascular diseases and hepatic steatosis.

13

324   *De novo* fatty acid synthesis from carbohydrates requires an adequate supply in metabolic

325   substrates, especially citrate that is produced by the TCA cycle from incoming pyruvate. The

326   glycolytic entry point into the TCA cycle is controlled by PDH and PC that convert pyruvate into

327   acetyl-CoA or OAA, respectively. Our data revealed that in addition to the increased production

328   of pyruvate from glucose, PC activity is increased whereas PDH is inhibited. This suggests that

329   pyruvate metabolism is rebalanced in favor of OAA in Huh7-*GCK⁺/HK2⁻* cells, as described in

330   healthy liver. Such a mechanism of anaplerosis is known to replenish TCA cycle intermediates and

331   compensate citrate export out of the mitochondria for lipogenesis fueling. Increased PC activity

332   is observed in both normal and pathological situations, mainly as a result of an increased

333   transcription of the PC gene. In our model, mRNA and protein levels were not affected, indicating

334   that PC activity can be regulated by alternative mechanisms depending on HK isoenzyme

335   expression. This may relate to lower levels of oxalate, a known inhibitor of PC activity, in Huh7-

336   *GCK⁺/HK2⁻* cells (Fig. 5c and Fig. 7 discussed below).

337   A rebalanced pyruvate usage in favor of OAA is also described for instance in SDH-deficient

338   neuroendocrine tumor cells, where succinate accumulates and PC activity is increased to maintain

339   OAA production, replenish the oxidative TCA cycle and support aspartate synthesis (29).

340   Interestingly, in comparison to Huh7 cells, succinate and aspartate levels are elevated in Huh7-

341   *GCK⁺/HK2⁻* where SDH activity is reduced, suggesting a direct link between PC and SDH activity in

342   hepatocytes. Several mechanisms inhibiting SDH have been described (38). Modification of the

343   expression of SDH subunits is unlikely as no variation was observed at the transcriptomic level*.*

344   Itaconate is a weak inhibitor of SDH produced by IRG1 from aconitate but this metabolite was not

345   detected and IRG1 mRNA was absent from the transcriptome of both cell lines. Whether fumarate

346   or other metabolites are responsible for the reduced SDH activity in GCK-expressing cells remains

14

347 to be investigated. Finally, SDH-deficient cells and LPS-stimulated macrophages have been shown

348 to elicit a hypoxic-like phenotype through accumulation of large amounts of succinate and

349 stabilization of HIF-1α (39, 40). Despite an elevated succinate steady-state level in Huh7-

350 *GCK⁺/HK2⁻* compared to Huh7 cells, we observed no difference in HIF-1α stabilization neither at

351 basal level nor upon induction (Supplementary Fig. 10). This suggested that the reduction of SDH

352 activity in Huh7-*GCK⁺/HK2⁻* cells was not strong enough to induce such a pseudo-hypoxic

353 phenotype.

354 Our gene-centric metabolic analysis of transcriptomic data revealed a wide spreading of

355 metabolic modifications resulting from HK isoenzyme switch. Illustrating these modifications,

356 Figure 7 is an attempt to integrate the observed changes in central carbon metabolism and closely

357 connected metabolic pathways. In particular, decreased level of alanine and increased aspartate

358 concentration in Huh7-*GCK⁺/HK2⁻* cells could be an indirect effect of PC activation that uses

359 pyruvate for the synthesis of OAA. As a consequence, hepatic transaminases may balance

360 intracellular pools of OAA, aspartate, alanine and pyruvate. Glutamate and GABA levels were also

361 modified, thus supporting anaplerosis of the TCA cycle through glutamine consumption and the

362 GABA shunt pathway, respectively. We also observed lower levels of oxalate, an end-product of

363 glyoxylate degradation. In Huh7-*GCK⁺/HK2⁻ cells,* increased levels of the enzyme alanine-

364 glyoxylate and serine-pyruvate aminotransferase (AGXT) could account for this phenotype as it

365 converts alanine and glyoxylate into pyruvate and glycine, which is also increased. Interestingly,

366 high level of AGXT is a good prognostic marker for HCC (41). Consistently, it was found that oxalate

367 inhibits liver PC, resulting in reduced gluconeogenesis and lipogenesis (42, 43). Thus, a higher PC

368 activity could be explained by lower levels of oxalate in Huh7-*GCK⁺/HK2⁻* cells. We also observed

369 that isoleucine and valine levels increased while BCAT1 (branched chain amino acid transaminase

370   1) predominant transcripts decreased. This suggests a reduced catabolism of branched chain

371   amino acids in Huh7-$GCK^+/HK2^-$ cells. Again, low levels of BCAT1 is a good prognostic marker for

372   HCC and oral supplementation with branched chain amino acids has been shown to reduce the

373   risk of liver cancer in cirrhotic patients (44, 45). If some metabolic modifications seem to advocate

374   for the restoration of a normal hepatocyte phenotype following the replacement of HK2 by GCK,

375   it cannot be a general statement. Indeed, the urea cycle was also impacted in Huh7-$GCK^+/HK2^-$

376   cells with lower levels of CPS1 and OTC, which are also observed in aggressive HCC tumors (46).

377   Altogether, our results demonstrate the broad impact of replacing HK2 by GCK in HCC cells, and

378   the key role played by the HK isoenzyme switch in HCC tumor metabolism.

379   We discovered that HK isoenzyme expression not only controls hepatic metabolic functions but

380   also interferes with intrinsic innate immunity of hepatocytes and antitumor immune surveillance.

381   Several reports have recently established functional links between glucose metabolism and

382   signaling pathways downstream of innate immunity sensors of the RLR family, RIG-I and MDA5

383   (47–49), which are usually associated with antiviral responses. However, RIG-I expression is

384   downregulated in hepatic cancer tissues and low RIG-I expression is correlated with poor survival

385   of patients, whereas RIG-I expression in HCC cell lines enhanced IFN response and cancer cell

386   apoptosis (34). This suggests an unexpected role of this receptor family in the antitumor response.

387   Here we show that Huh7 cells expressing GCK instead of HK2 exhibit a higher sensitivity to RIG-I

388   and MDA5 ligands, and produce higher levels of type I/III IFNs and inflammatory cytokines. This

389   immune phenotype occurs in a context of reduced SDH activity and increased intracellular content

390   in succinate (Fig. 5l-m). A pro-inflammatory function of immune cells such as macrophages was

391   previously linked to TCA rewiring, with reduced SDH activity resulting in succinate accumulation

392   (39, 50, 51). Succinate can also be secreted from LPS-activated macrophages and activate its

393   cognate receptor, succinate receptor 1 (SUCNR1, previously known as GPR91) in an autocrine and

394   paracrine manner to further enhance production of IL-1β (52). Interestingly, glucose metabolism

395   promotes RIG-I and MDA5 signaling through the O-GlcNAcylation of the mitochondrial adaptor

396   MAVS (47). Thus, an intriguing hypothesis is that GCK expression could facilitate MAVS signaling

397   by increasing UDP-GlcNAc through upregulation of the hexosamine biosynthetic pathway. HK2

398   binding at the surface of mitochondria may also compete with pyruvate carboxylase, metabolites

399   or mitochondria factors known to control MAVS signaling (47–49). Here we show that HK2

400   knockdown promotes RIG-I-induced ISRE-dependent transcription (Fig. 6d). This is consistent with

401   the results obtained by Zhang W. et al. (48), indicating that HK2 interaction with MAVS restrains

402   RIG-I-induced IFN-β secretion. Further investigations are now required to decipher the molecular

403   links between metabolism and immune responses.

404   Beyond the inhibition of RLR signaling, other mechanisms might contribute to tumor escape from

405   immune surveillance in HCC patients. In advanced-stage HCC patients, NK cells often exhibit

406   reduced infiltration and impaired functional activities (53). We thus compared the sensitivity of

407   Huh7-$GCK^+/HK2^-$ cells to Huh7, and found that sensitivity to NK cell lysis is restored when HK2 is

408   replaced by GCK. When analyzing cell surface expression of the NK cells inhibitors, HLA class I and

409   MICA/B, no significant changes were observed between cell lines (Supplementary Fig. 9). In

410   contrast, an increased transcription and surface expression of ICAM1 (FC=2.6; Supplementary Fig.

411   9) was observed in Huh7-$GCK^+/HK2^-$. Since ICAM-1 binding to active LFA-1 at the surface of NK

412   cells is essential for granule polarization and efficient killing of the target cells (54), its enhanced

413   exposition at the surface of Huh7-$GCK^+/HK2^-$ may contribute to their higher sensitivity to NK cell-

414   mediated killing. These results suggest that HK2 expression at the expense of GCK in HCC tumors

415   decreases immune responsiveness and sensitivity to NK cytotoxicity, thus favoring immune

416   escape.

417   Taken together, our data demonstrate that beyond glycolysis, the hexokinase isoenzyme switch

418   in an HCC model rewires central carbon metabolism, promotes lipogenesis, enhances innate

419   immune functions, and restores sensitivity to natural killer cells.

420

Materials and Methods

421
422
423   **Materials.** Unless otherwise specified, chemicals were from Merck Sigma-Aldrich. The RIG-I

424   specific ligand 3p-hpRNA and the MDA5/TLR3 ligand poly(I:C) HMW (High Molecular Weight) were

425   from Invivogen.

426   **Cell cultures.** Huh7 cells and derivatives were grown as previously described (55) in DMEM, 10%

427   fetal calf serum (FCS), penicillin/streptomycin, 1 mM pyruvate, 2 mM L-glutamine. Culture

428   medium and additives were from Gibco except FCS (Dominique Dutcher).

429   **Cell lines**. 15×10^4 Huh7 cells were transduced for GCK expression at different multiplicities of

430   infection (lentiviral transduction using the pLEX-GCK construct). The Huh7-$GCK^+/HK2^+$ cells were

431   then cultured for 7 days with puromycin (1 µg/mL) before amplification. HK2 knock-out was

432   achieved using the CRISPR/Cas9 system as previously described (56) to obtain Huh7-$GCK^+/HK2^-$

433   cells. A single guide RNA (sgRNA) pair was designed for double nicking using the CRISPR Design

434   Tool (http://tools.genome-engineering.org). The guide sequence oligos (sgRNA$_1$(*HK2*): 5'-

435   CACCGTGACCACATTGCCGAATGCC-3' and sgRNA$_2$(*HK2*): 5'-CACCGTTACCTCGTCTAGTTTAGTC-3')

436   were cloned into a plasmid containing sequences for Cas9 expression and the sgRNA scaffold

437   (pSpCas9(BB)-2A-GFP, Addgene plasmid #48138). 48 h post-transfection, cells were sorted by

438 FACS based on the transient expression of GFP and cloned by limiting dilution. Effective deletion

439 of HK2 was assessed by qPCR.

440 For *HK2* knock-down, Huh7-*GCK+/HK2+* cells were transduced with lentiviral vectors expressing

441 HK2-targeting shRNAs, and antibiotic selection was applied (hygromycin; 100 µg/ml). The *HK2-*

442 targeting sequence 5'-

443 CCGGCCAGAAGACATTAGAGCATCTCTCGAGAGATGCTCTAATGTCTTCTGGTTTTTT-3' was cloned in

444 the pLKO.1 hygro vector (a gift from Bob Weinberg; Addgene plasmid #24150). HK2 expression in

445 Huh7-*GCK+/HK2+* and Huh7-*GCK+/HK2-Sh* was analyzed on cell lysates by western blotting

446 (Supplementary Fig. 8).

447 **Enzymatic activity assays.** Cells were trypsinized, washed twice, and cell pellets were stored at -

448 80°C. Protein extractions and assays were performed as previously described for hexokinase (57–

449 59) and pyruvate carboxylase (60). Specific enzymatic assays are described in Supplementary

450 Methods.

451 **Metabolomics profiling.** Cells were seeded at 13×10^5 cells in $75 cm^2$ dishes. After 24 h, culture

452 medium was replaced and cells were further incubated during 24 h. Culture supernatants were

453 collected and stored at -80°C. Cells were harvested, washed twice with ice-cold PBS, and cell

454 pellets were stored at -80°C. To analyze catabolic glucose flux, cells were incubated with [U-^{13}C]-

455 glucose (Sigma-Aldrich; 389374-2G) at 12.5 mM and unlabeled glucose at 12.5 mM for 24h.

456 Extraction, separation and analysis of the metabolites by GC-MS are described in Supplementary

457 Methods.

458 **Transcriptome profiling of Huh7 and Huh7-*GCK+/HK2-* cell lines.** Transcriptome profiling was

459 performed by next generation sequencing (Profilexpert, Lyon). To identify differentially expressed

460 genes, raw data were processed using the DESeq2 analysis pipeline (61). See Supporting

19

461   Information and Gene Expression Omnibus database with the accession number GSE144214 for

462   entire raw data.

463   **Pathway analysis.** The list of transcripts differentially expressed in Huh7 and Huh7-GCK^+/$HK2^-$ cell

464   lines was analyzed by gene set enrichment analysis (IPA, Build version: 486617M, Qiagen)

465   weighted by their corresponding fold-change and *p* value. The fold-change cut-off of mean

466   expression for each transcript was set at 2 with an adjusted *p* value<0.05. The list of genes

467   associated with "Type I-IFN signaling pathway" was defined in the AmiGO 2 database. Expression

468   data of these genes were retrieved from the transcriptomes of Huh7-GCK^+/$HK2^-$ and Huh7, and

469   correspond for each gene to the most differentially expressed transcript.

470   **Cell migration assay.** $2x10^4$ cells were plated in the upper chamber of transwells (Sarstedt, PET

471   8.0-µm, TL - 833932800) with DMEM without FCS to allow migration for 24 h at 37°C. DMEM with

472   10% FCS was distributed in each well, below the chamber. Chambers were gently picked up before

473   a brief PBS rinse and 0.05% crystal violet coloration. The migrated cells were analyzed a Leica M50

474   microscope using a magnification factor of 20x. The number of cells that have migrated through

475   the membrane and attached on the underside of the membrane were counted using the software

476   Image J.

477   **Respiration Assay.** Respiration was measured using an Extracellular Flux Analyzer (Seahorse

478   Bioscience). The assay was performed according to the Agilent Seahorse XF Cell Mito Stress Test

479   as detailed in Supplementary Methods. The number of cells was determined at the end of the run

480   using the SRB assay as previously described (62) or in plate cell counting by Cytation 1 imaging

481   reader (Biotek).

482   **Intracellular lipid staining.** For microscopic observations, cells were fixed 48 h post-seeding, and

483   intracellular lipids stained with Oil-Red-O as described in Supplementary Methods. For the

484 quantification of intracellular lipid droplets by FACS, cells were stained with the 4,4-difluoro-

485 1,3,5,7,8-Pentamethy-4-Bora-3a,4a-Diaza-s-indacene (BODIPY) 493/503 dye (Tocris Bio-Techne).

486 **Protein, ApoB, and Lipid Quantification**. Protein concentration was determined using the DC

487 Protein Assay (Bio-Rad). ApoB concentration in medium and gradients fractions was determined

488 by ELISA as previously described (63). Total concentrations of cholesterol, phospholipids, and

489 triglycerides (TG) were determined using specific assays from Millipore Sigma-Aldrich (ref.

490 MAK043, MAK122 and MAK266 respectively). Free Fatty Acids were quantified using a specific

491 assay kit from Abcam (ref. ab65341).

492 **Iodixanol density gradients.** Iodixanol gradients were prepared as previously described (64). One

493 ml of culture supernatant was applied to the top of 6 to 56% iodixanol gradients and centrifuged

494 for 10h at 41,000rpm and 4°C in a SW41 rotor. The gradient was harvested by tube puncture from

495 the bottom and collected into 22 fractions (0.5 ml each). The density of each fraction was

496 determined by weighing.

497 **Metabolic network coherence computational analysis.** In order to measure the consistency of

498 differentially expressed genes with a metabolic network, we employed the metabolic network

499 coherence measure introduced by Sonnenschein *et al.* (65) (see Supplementary Methods for

500 details). This approach was previously applied to various disease-related transcriptome profiles

501 (66, 67) and for extracting information on the genetic control of metabolic organization (68).

502 Recently, detailed theoretical analysis of the extended version of the method has been performed

503 by Nyczka and Hütt (69)

504 **Western-Blot Analysis.** Protein expression was determined by standard western-blot analysis

505 (See Supplementary Methods for details).

506 **RLR stimulation**

507   Cells were seeded in 96-well or 24-well plates. After 24 h, cells were co-transfected with indicated

508   doses of the RIG-I ligand 3p-hpRNA or the MDA5/TLR3 ligand poly(I:C) HMW together with the

509   pISRE-luc (1.25 μg/ml) and pRL-SV40 (0.125 μg/ml) reporter plasmids using the JetPEI-Hepatocyte

510   reagent (Polyplus Transfection). Manufacturer's instructions were followed. After 48 h,

511   supernatants were collected for cytokine quantification. Firefly and Renilla luciferase expressions

512   within cells were determined using the Dual-Glo luciferase Assay system (Promega) and an Infinite

513   M200 microplate reader (TECAN).

514   **Cytokine assays**

515   Clarified culture supernatants were collected and stored at -20°C. IL-8 was quantified using the

516   Cytometric Bead Array for human IL-8 (BD Biosciences). Other cytokines were assayed using the

517   LEGENDPlex multiplex assay (Human Anti-Virus Response Panel, BioLegend). Fluorescence was

518   analyzed using a FACS Canto II (BD Biosciences).

519   **NK cell cytotoxicity test**

520   NK cells were isolated as described in Supplementary Methods from human buffy coats of healthy

521   donors obtained from the Etablissement Français du Sang. Informed consent was obtained from

522   donors and experimental procedures were approved by the local institutional review committee.

523   Huh7 or Huh7-$GCK^+/HK2^-$ were seeded at $1x10^5$ cells per well in a 24-well plate in RPMI-1640

524   (Gibco) with 10% FCS and 40 μg/ml gentamycin. After 24 h, $3x10^5$ or $3x10^6$ NK cells were added

525   to the culture wells. The cytotoxicity assay was performed for 4 h at 37°C, under 5% CO_2. Target

526   hepatoma cells were harvested after trypsination, labelled with propidium iodide (PI) and

527   analyzed by FACS. Cell death was monitored after morphological gating on hepatocytes.

528   **Statistics and reproducibility**

22

529 All the statistical analyses were performed with GraphPad Prism or Analyse-it softwares. Details

530 of statistical analyses can be found in figure legends.

531 **Acknowledgments**

532

543 **Author Contributions**

544 L.P-C., P-O.V., O.D., V.L. designed the experiments with critical advices from G.J.P.R., P.A., R.R. and
545 F.V.F.; C.J., A.A-G., K.O., B.P., G.J.P.R., N.A, R.R. and F.V.F. performed experiments and analyzed
546 the data; P.N. and M-T.H. performed metabolic network computational analysis; L.P-C., P-O.V.,
547 P.A., F.V.F, V.L. and O.D. analyzed the data, prepared figures and wrote the manuscript.

548

549 **References**

550

551 1. A. Villanueva, Hepatocellular Carcinoma. *N. Engl. J. Med.* **380**, 1450–1462 (2019).

552 2. M. Kudo, *et al.*, Lenvatinib versus sorafenib in first-line treatment of patients with
553 unresectable hepatocellular carcinoma: a randomised phase 3 non-inferiority trial. *The*
554 *Lancet* **391**, 1163–1173 (2018).

555 3. J. M. Llovet, R. Montal, D. Sia, R. S. Finn, Molecular therapies and precision medicine for
556 hepatocellular carcinoma. *Nat Rev Clin Oncol* **15**, 599–616 (2018).

557   4.   S. De Matteis, *et al.*, Aberrant Metabolism in Hepatocellular Carcinoma Provides
558   Diagnostic and Therapeutic Opportunities. *Oxidative Medicine and Cellular Longevity* **2018**,
559   1–13 (2018).

560   5.   F. V. Filipp, *et al.*, Glutamine-fueled mitochondrial metabolism is decoupled from glycolysis
561   in melanoma. *Pigment Cell & Melanoma Research* **25**, 732–739 (2012).

562   6.   N. Hay, Reprogramming glucose metabolism in cancer: can it be exploited for cancer
563   therapy? *Nat Rev Cancer* **16**, 635–649 (2016).

564   7.   M. G. Vander Heiden, L. C. Cantley, C. B. Thompson, Understanding the Warburg effect:
565   the metabolic requirements of cell proliferation. *Science* **324**, 1029–1033 (2009).

566   8.   J. Jiang, P. Nilsson-Ehle, N. Xu, Influence of liver cancer on lipid and lipoprotein
567   metabolism. *Lipids Health Dis* **5**, 4 (2006).

568   9.   D. DeWaal, *et al.*, Hexokinase-2 depletion inhibits glycolysis and induces oxidative
569   phosphorylation in hepatocellular carcinoma and sensitizes to metformin. *Nature
570   Communications* **9**, 446 (2018).

571   10. C. Guo, *et al.*, Coordinated regulatory variation associated with gestational hyperglycaemia
572   regulates expression of the novel hexokinase HKDC1. *Nat Commun* **6**, 6069 (2015).

573   11. G. Guzman, *et al.*, Evidence for Heightened Hexokinase II Immunoexpression in
574   Hepatocyte Dysplasia and Hepatocellular Carcinoma. *Dig Dis Sci* **60**, 420–426 (2015).

575   12. A. J. Wolf, *et al.*, Hexokinase Is an Innate Immune Receptor for the Detection of Bacterial
576   Peptidoglycan. *Cell* **166**, 624–636 (2016).

577   13. V. P. Tan, S. Miyamoto, HK2/hexokinase-II integrates glycolysis and autophagy to confer
578   cellular protection. *Autophagy* **11**, 963–964 (2015).

579   14. D. J. Roberts, V. P. Tan-Sah, E. Y. Ding, J. M. Smith, S. Miyamoto, Hexokinase-II Positively
580   Regulates Glucose Starvation-Induced Autophagy through TORC1 Inhibition. *Mol. Cell* **53**,
581   521–533 (2014).

582   15. M. Kishore, *et al.*, Regulatory T Cell Migration Is Dependent on Glucokinase-Mediated
583   Glycolysis. *Immunity* **47**, 875-889.e10 (2017).

584   16. N. C. W. Lee, M. A. Carella, S. Papa, C. Bubici, High Expression of Glycolytic Genes in
585   Cirrhosis Correlates With the Risk of Developing Liver Cancer. *Front Cell Dev Biol* **6**, 138
586   (2018).

587   17. M. Uhlén, *et al.*, Tissue-based map of the human proteome. *Science* **347** (2015).

588   18. M. Uhlen, *et al.*, A pathology atlas of the human cancer transcriptome. *Science* **357** (2017).

589   19.   J.-J. Yoo, *et al.*, Hexokinase-II Inhibition Synergistically Augments the Anti-tumor Efficacy of
590   Sorafenib in Hepatocellular Carcinoma. *Int J Mol Sci* **20** (2019).

591   20.   C. M. Porter, B. G. Miller, Cooperativity in monomeric enzymes with single ligand-binding
592   sites. *Bioorganic Chemistry* **43**, 44–50 (2012).

593   21.   M. Larion, R. K. Salinas, L. Bruschweiler-Li, B. G. Miller, R. Brüschweiler, Order–Disorder
594   Transitions Govern Kinetic Cooperativity and Allostery of Monomeric Human Glucokinase.
595   *PLoS Biology* **10**, e1001452 (2012).

596   22.   I. Thiele, *et al.*, A community-driven global reconstruction of human metabolism. *Nat.*
597   *Biotechnol.* **31**, 419–425 (2013).

598   23.   D. C. Zielinski, *et al.*, Pharmacogenomic and clinical data link non-pharmacokinetic
599   metabolic dysregulation to drug side effect pathogenesis. *Nature Communications* **6**, 7101
600   (2015).

601   24.   G. van den Berghe, The role of the liver in metabolic homeostasis: Implications for inborn
602   errors of metabolism. *Journal of Inherited Metabolic Disease* **14**, 407–420 (1991).

603   25.   J. M. Berg, J. L. Tymoczko, L. Stryer, Each Organ Has a Unique Metabolic Profile.
604   *Biochemistry. 5th edition* (2002) (January 13, 2020).

605   26.   F. Beilstein, *et al.*, Lysophosphatidylcholine acyltransferase 1 is downregulated by hepatitis
606   C virus: impact on production of lipo-viro-particles. *Gut* **66**, 2160–2169 (2017).

607   27.   H. N. Ginsberg, LIPOPROTEIN PHYSIOLOGY. *Endocrinology and Metabolism Clinics of North*
608   *America* **27**, 503–519 (1998).

609   28.   S. J. R. Meex, U. Andreo, J. D. Sparks, E. A. Fisher, Huh-7 or HepG2 cells: which is the better
610   model for studying human apolipoprotein-B100 assembly and secretion? *J. Lipid Res.* **52**,
611   152–158 (2011).

612   29.   C. Lussey-Lepoutre, *et al.*, Loss of succinate dehydrogenase activity results in dependency
613   on pyruvate carboxylation for cellular anabolism. *Nat Commun* **6**, 8784 (2015).

614   30.   V. Lampropoulou, *et al.*, Itaconate Links Inhibition of Succinate Dehydrogenase with
615   Macrophage Metabolic Remodeling and Regulation of Inflammation. *Cell Metab.* **24**, 158–
616   166 (2016).

617   31.   A. Mansouri, C.-H. Gattolliat, T. Asselah, Mitochondrial Dysfunction and Signaling in
618   Chronic Liver Diseases. *Gastroenterology* **155**, 629–647 (2018).

619   32.   E. L. Mills, B. Kelly, L. A. J. O'Neill, Mitochondria are the powerhouses of immunity. *Nature*
620   *Immunology* **18**, 488 (2017).

621   33.   M. Cheng, *et al.*, Stat1 mediates an auto-regulation of hsp90β gene in heat shock
622   response. *Cellular Signalling* **22**, 1206–1213 (2010).

25

623   34.   J. Hou, *et al.*, Hepatic RIG-I predicts survival and interferon-α therapeutic response in
624   hepatocellular carcinoma. *Cancer Cell* **25**, 49–63 (2014).

625   35.   G. Panasyuk, *et al.*, PPARγ contributes to PKM2 and HK2 expression in fatty liver. *Nat*
626   *Commun* **3**, 672 (2012).

627   36.   O. A. Mesarwi, *et al.*, Hepatocyte Hypoxia Inducible Factor-1 Mediates the Development of
628   Liver Fibrosis in a Mouse Model of Nonalcoholic Fatty Liver Disease. *PLoS One* **11** (2016).

629   37.   D. J. Roberts, S. Miyamoto, Hexokinase II integrates energy metabolism and cellular
630   protection: Akting on mitochondria and TORCing to autophagy. *Cell Death and*
631   *Differentiation* **22**, 248–257 (2015).

632   38.   J. Van den Bossche, L. A. O'Neill, D. Menon, Macrophage Immunometabolism: Where Are
633   We (Going)? *Trends in Immunology* **38**, 395–406 (2017).

634   39.   G. M. Tannahill, *et al.*, Succinate is an inflammatory signal that induces IL-1β through HIF-
635   1α. *Nature* **496**, 238–242 (2013).

636   40.   K. Kluckova, D. A. Tennant, Metabolic implications of hypoxia and pseudohypoxia in
637   pheochromocytoma and paraganglioma. *Cell Tissue Res.* **372**, 367–378 (2018).

638   41.   Y. Sun, *et al.*, Loss of alanine-glyoxylate and serine-pyruvate aminotransferase expression
639   accelerated the progression of hepatocellular carcinoma and predicted poor prognosis. *J*
640   *Transl Med* **17**, 390 (2019).

641   42.   E. A. Yount, R. A. Harris, Studies on the inhibition of gluconeogenesis by oxalate. *Biochim.*
642   *Biophys. Acta* **633**, 122–133 (1980).

643   43.   I. E. O'Neill, D. W. Bannister, The effects of oxalate and glucose on lipogenesis by isolated
644   hepatocytes from normal and biotin-deficient chicks (Gallus domesticus). *Int. J. Biochem.*
645   **16**, 517–521 (1984).

646   44.   Y. Muto, *et al.*, Overweight and obesity increase the risk for liver cancer in patients with
647   liver cirrhosis and long-term oral supplementation with branched-chain amino acid
648   granules inhibits liver carcinogenesis in heavier patients with liver cirrhosis. *Hepatol. Res.*
649   **35**, 204–214 (2006).

650   45.   T. Kawaguchi, *et al.*, Branched-chain amino acids prevent hepatocarcinogenesis and
651   prolong survival of patients with cirrhosis. *Clin. Gastroenterol. Hepatol.* **12**, 1012-1018.e1
652   (2014).

653   46.   A. Ally, *et al.*, Comprehensive and Integrative Genomic Characterization of Hepatocellular
654   Carcinoma. *Cell* **169**, 1327-1341.e23 (2017).

655   47.   T. Li, *et al.*, O-GlcNAc Transferase Links Glucose Metabolism to MAVS-Mediated Antiviral
656   Innate Immunity. *Cell Host Microbe* **24**, 791-803.e6 (2018).

657   48.   W. Zhang, *et al.*, Lactate Is a Natural Suppressor of RLR Signaling by Targeting MAVS. *Cell*
658   **178**, 176-189.e15 (2019).

659   49.   Z. Cao, *et al.*, Pyruvate Carboxylase Activates the RIG-I-like Receptor-Mediated Antiviral
660   Immune Response by Targeting the MAVS signalosome. *Sci Rep* **6**, 22002 (2016).

661   50.   L. A. J. O'Neill, A Broken Krebs Cycle in Macrophages. *Immunity* **42**, 393–394 (2015).

662   51.   E. L. Mills, *et al.*, Succinate Dehydrogenase Supports Metabolic Repurposing of
663   Mitochondria to Drive Inflammatory Macrophages. *Cell* **167**, 457-470.e13 (2016).

664   52.   A. Littlewood-Evans, *et al.*, GPR91 senses extracellular succinate released from
665   inflammatory macrophages and exacerbates rheumatoid arthritis. *J. Exp. Med.* **213**, 1655–
666   1662 (2016).

667   53.   L. Cai, *et al.*, Functional impairment in circulating and intrahepatic NK cells and relative
668   mechanism in hepatocellular carcinoma patients. *Clin. Immunol.* **129**, 428–437 (2008).

669   54.   Y. T. Bryceson, M. E. March, D. F. Barber, H.-G. Ljunggren, E. O. Long, Cytolytic granule
670   polarization and degranulation controlled by different receptors in resting NK cells. *J Exp*
671   *Med* **202**, 1001–1012 (2005).

672   55.   C. Scholtes, *et al.*, Enhancement of genotype 1 hepatitis C virus replication by bile acids
673   through FXR. *J. Hepatol.* **48**, 192–199 (2008).

674   56.   F. A. Ran, *et al.*, Genome engineering using the CRISPR-Cas9 system. *Nature Protocols* **8**,
675   2281–2308 (2013).

676   57.   Y. Kuang, S. J. Schomisch, V. Chandramouli, Z. Lee, Hexokinase and glucose-6-phosphatase
677   activity in woodchuck model of hepatitis virus-induced hepatocellular carcinoma. *Comp.*
678   *Biochem. Physiol. C Toxicol. Pharmacol.* **143**, 225–231 (2006).

679   58.   C. Ramière, *et al.*, Activity of hexokinase is increased by its interaction with hepatitis C
680   virus protein NS5A. *J. Virol.* **88**, 3246–3254 (2014).

681   59.   L. Perrin-Cocon, *et al.*, Toll-like Receptor 4-Induced Glycolytic Burst in Human Monocyte-
682   Derived Dendritic Cells Results from p38-Dependent Stabilization of HIF-1α and Increased
683   Hexokinase II Expression. *J. Immunol.* **201**, 1510–1521 (2018).

684   60.   J. Payne, J. G. Morris, Pyruvate carboxylase in Rhodopseudomonas spheroides. *J. Gen.*
685   *Microbiol.* **59**, 97–101 (1969).

686   61.   M. I. Love, W. Huber, S. Anders, Moderated estimation of fold change and dispersion for
687   RNA-seq data with DESeq2. *Genome Biology* **15**, 550 (2014).

688   62.   P. Skehan, *et al.*, New colorimetric cytotoxicity assay for anticancer-drug screening. *J. Natl.*
689   *Cancer Inst.* **82**, 1107–1112 (1990).

690   63.   C. Scholtes, *et al.*, High plasma level of nucleocapsid-free envelope glycoprotein-positive
691   lipoproteins in hepatitis C patients. *Hepatology* **56**, 39–48 (2012).

692   64.   V. Icard, *et al.*, Secretion of hepatitis C virus envelope glycoproteins depends on assembly
693   of apolipoprotein B positive lipoproteins. *PLoS ONE* **4**, e4233 (2009).

694   65.   N. Sonnenschein, M. Geertz, G. Muskhelishvili, M.-T. Hütt, Analog regulation of metabolic
695   demand. *BMC Syst Biol* **5**, 40 (2011).

696   66.   N. Sonnenschein, *et al.*, A network perspective on metabolic inconsistency. *BMC Syst Biol*
697   **6**, 41 (2012).

698   67.   C. Knecht, C. Fretter, P. Rosenstiel, M. Krawczak, M.-T. Hütt, Distinct metabolic network
699   states manifest in the gene expression profiles of pediatric inflammatory bowel disease
700   patients and controls. *Sci Rep* **6**, 32584 (2016).

701   68.   K. Schlicht, *et al.*, The metabolic network coherence of human transcriptomes is associated
702   with genetic variation at the cadherin 18 locus. *Hum. Genet.* **138**, 375–388 (2019).

703   69.   P. Nyczka, M.-T. Hütt, Generative network model of transcriptome patterns in disease
704   cohorts with tunable signal strength. *Phys. Rev. Research* **2**, 033130 (2020).

705   70.   J. Gao, *et al.*, Integrative Analysis of Complex Cancer Genomics and Clinical Profiles Using
706   the cBioPortal. *Sci Signal* **6**, pl1 (2013).

707   71.   E. Cerami, *et al.*, The cBio Cancer Genomics Portal: An Open Platform for Exploring
708   Multidimensional Cancer Genomics Data. *Cancer Discov* **2**, 401–404 (2012).

709

710   **Figures**
711

a **HK1 expression**
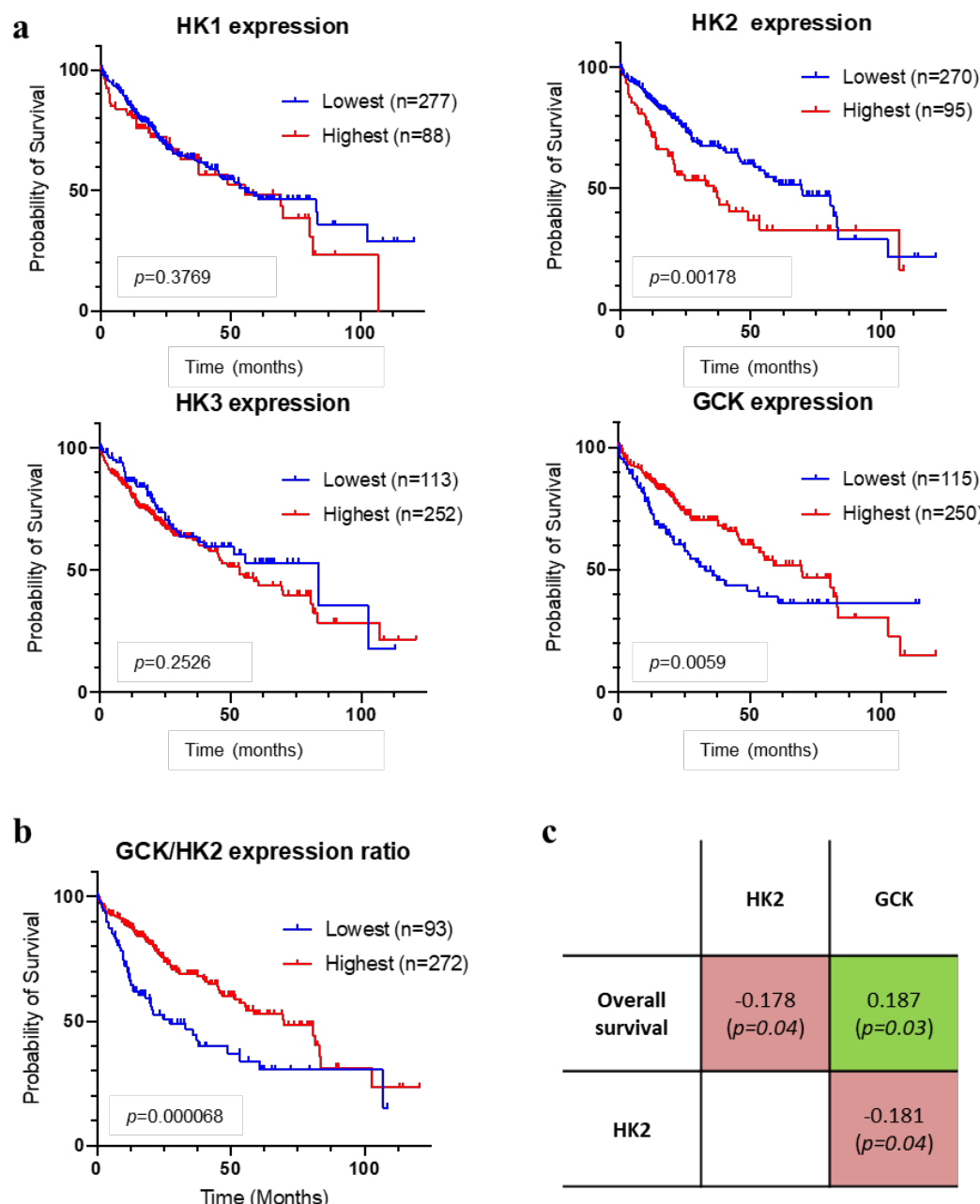
HK2 expression

Figure 1. Correlation between hexokinase expression levels in HCC tumors and patient survival.
713   **a** Kaplan–Meier estimates of the survival of HCC patients depending on the expression of HK1,
714   HK2, HK3 and GCK (HK4) genes in tumor biopsies (n=365; TCGA expression data retrieved from
715   cBioPortal)(70, 71). Duplicate analyses from the same patient were removed as well as patients
716   who died when biopsied (overall survival=0 months). Optimal stratification based on highest and
717   lowest gene expression values was determined using Protein Atlas database (18). **b** Same as above
718   but patients were stratified based on the GCK/HK2 gene expression ratio. The stratification
719   showing the lowest *p* value when comparing subgroups of patients with the highest to the lowest

29

720   GCK/HK2 expression ratio is displayed. Patient TCGA-DD-AAE9 exhibiting undetectable levels of
721   GCK and HK2 was removed from this analysis as the GCK/HK2 ratio could not be calculated. **c**
722   Correlations between patient survival, GCK expression and HK2 expression. Spearman's rank
723   correlation test on the subset 130 patients for whom the period between diagnosis and death is
724   precisely known (uncensored data).

725

726

727
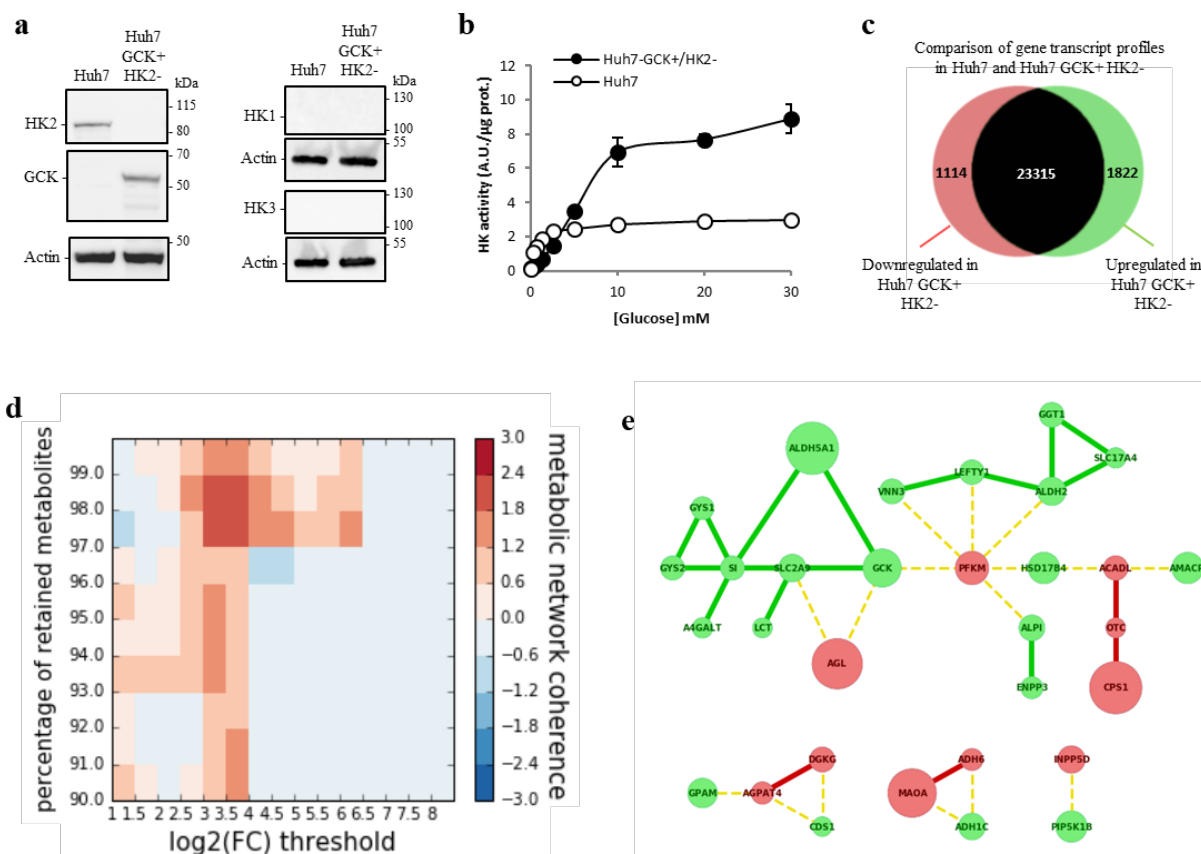
728   **Figure 2. Hexokinase isoenzyme switch in Huh7 cells induces extended modifications of**
729   **metabolic connections. a** Western-blot analysis of HK1, HK2, HK3 and GCK expression in Huh7
730   and Huh7-$GCK^+/HK2^-$. **b** Hexokinase activity in homogenates of Huh7 and Huh7-$GCK^+/HK2^-$ cells. **c**
731   Number of genes changing their expression pattern in Huh7 and Huh7-$GCK^+/HK2^-$ cells (see
732   Supplementary Table 2 for details). **d** Heatmap showing clustering enrichment scores of the
733   networks obtained when mapping differentially expressed genes to the human metabolic model
734   Recon2. Clustering enrichment scores from the highest in red to the lowest in blue were
735   calculated for different gene expression thresholds (Log$_2$|FC|) and percentages of retained
736   currency metabolites. **e** Gene network corresponding to the maximal clustering enrichment score
737   (Log$_2$|FC|>3; removed currency metabolites = 2%). The transcription of nodes in green was
738   upregulated and those in red downregulated in Huh7-$GCK^+/HK2^-$ compared to Huh7 cells. Plain

739 edges mark coregulation between nodes and broken edges inverse regulation at the
740 transcriptional level.
741
742

a

Molecular and Cellular Functions		
Name	*p*-value range	Number of genes involved
Cellular Movement	$7.68 \times 10^{-6} - 4.66 \times 10^{-25}$	701
Lipid Metabolism	$2.00 \times 10^{-6} - 3.12 \times 10^{-14}$	414
Molecular Transport	$5.63 \times 10^{-6} - 3.12 \times 10^{-14}$	361
Small Molecule Biochemistry	$5.63 \times 10^{-6} - 3.12 \times 10^{-14}$	462
Protein Synthesis	$1.87 \times 10^{-6} - 3.42 \times 10^{-14}$	199

b

Cellular Movement Functional Annotations		
Name	*p*-value	Number of genes involved
Migration of cells	4.66×10^{-25}	585
Cell movement	3.48×10^{-24}	642
Cell movement of blood cells	1.52×10^{-18}	276
Leucocyte migration	1.59×10^{-18}	274
Invasion of cells	5.33×10^{-17}	306

c

Lipid Metabolism Functional Annotations		
Name	*p*-value	Number of genes involved
Concentration of lipid	3.12×10^{-14}	256
Synthesis of lipid	2.37×10^{-10}	233
Fatty acid metabolism	4.31×10^{-10}	166
Quantity of steroid	4.48×10^{-09}	138
Concentration of cholesterol	6.58×10^{-08}	94

743
744
745 **Figure 3. Huh7-*GCK+/HK2-* cells have a higher migration capacity and lipid droplets content. a**
746 Analysis of differentially expressed genes in the two cell lines using gene set enrichment analysis
747 (|FC|>2 with a *p* value <0.05). Top five enriched molecular and cellular functions are presented.
748 **b** and **c** Ranked IPA-annotations associated with 'cellular movement' and 'lipid metabolism'. **d, e**

749   Results of transwell-migration tests. **d** Representative images and **e** count of migrating cells. **f** Oil
750   Red-O staining of lipid droplets (red) with nucleus counterstaining (blue). **g** Quantification of
751   intracellular lipids by FACS after BODIPY staining. E and G correspond to means ± SEM with n≥3
752   (*p* value determined by Student's t-test).
753

754
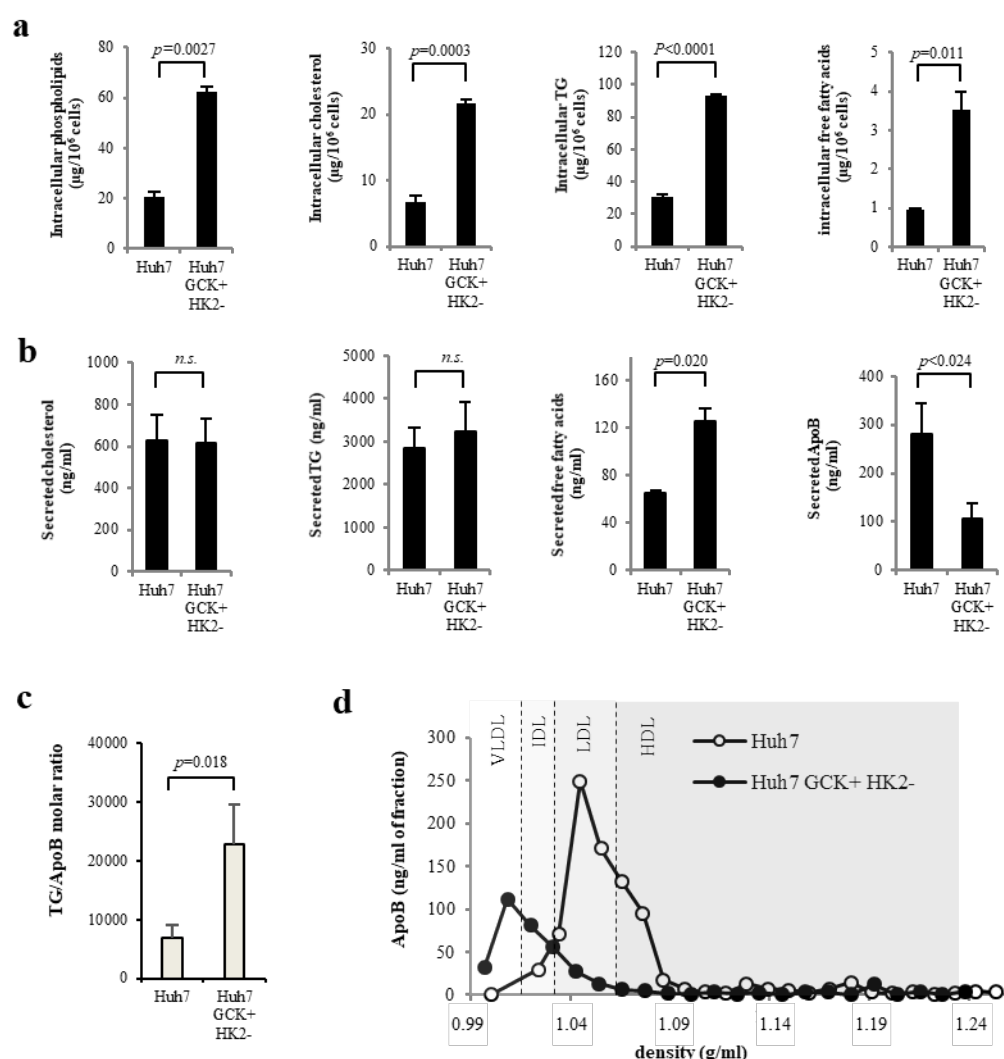
755   **Figure 4. Lipogenesis and very-low-density lipoproteins (VLDL) secretion are restored in Huh7-**
756   ***GCK⁺/HK2⁻* cells. a** Quantification of intracellular lipids in total cell extracts of Huh7 and Huh7-
757   *GCK⁺HK2⁻* cells. **b** Lipids and ApoB secretions in supernatants of cells cultured 24h without FCS. **c**
758   TG/ApoB molar ratio calculated from quantifications determined in b. **d** Supernatants of Huh7
759   and Huh7-*GCK⁺/HK2⁻* were analyzed by ultracentrifugation on iodixanol density gradients. ApoB
760   was quantified in each fraction by ELISA. Presented data correspond to means ± SEM (n≥3, *p* value
761   determined by Student's t-test) except for d) that shows one representative experiment.
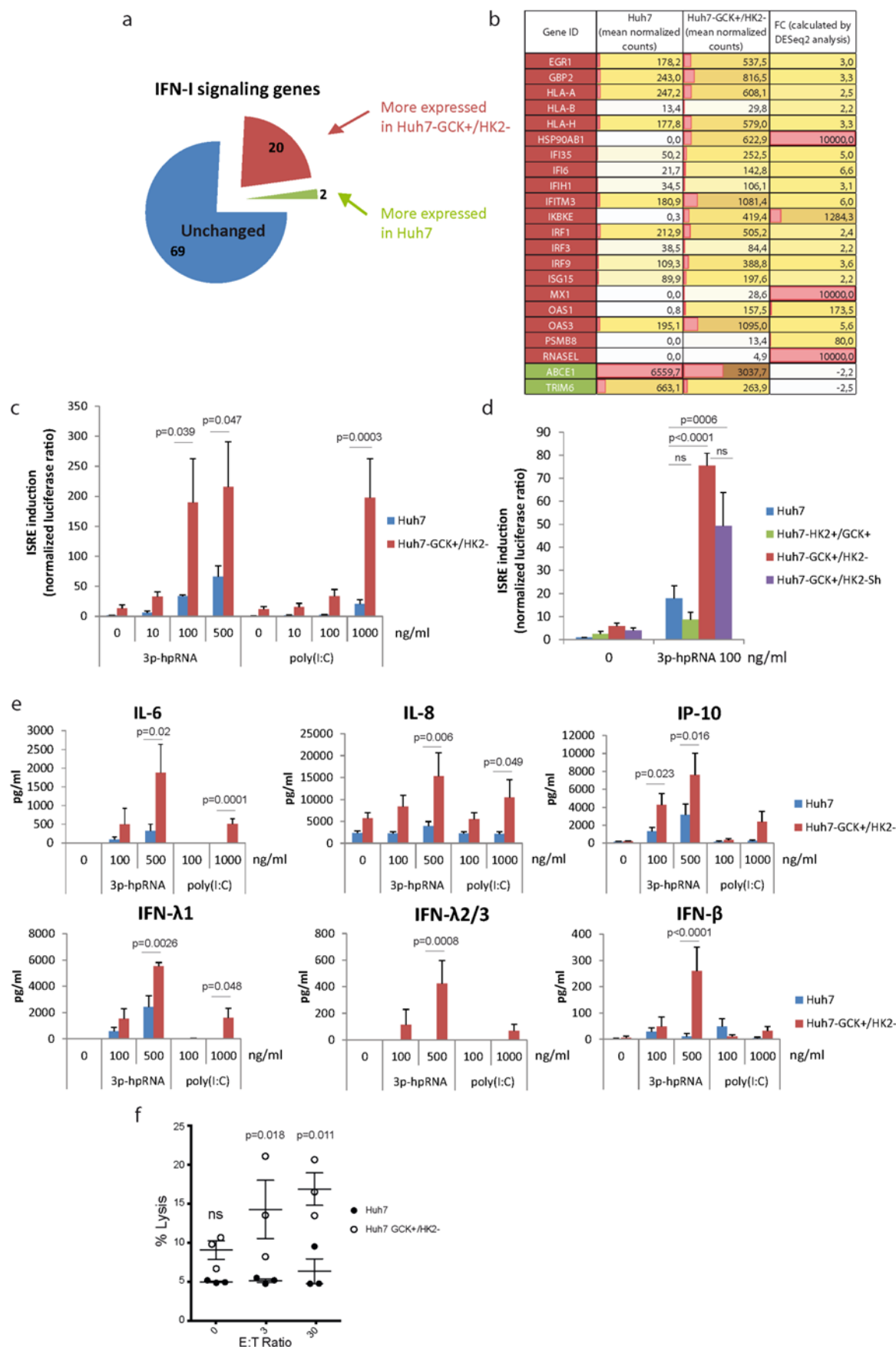762

763
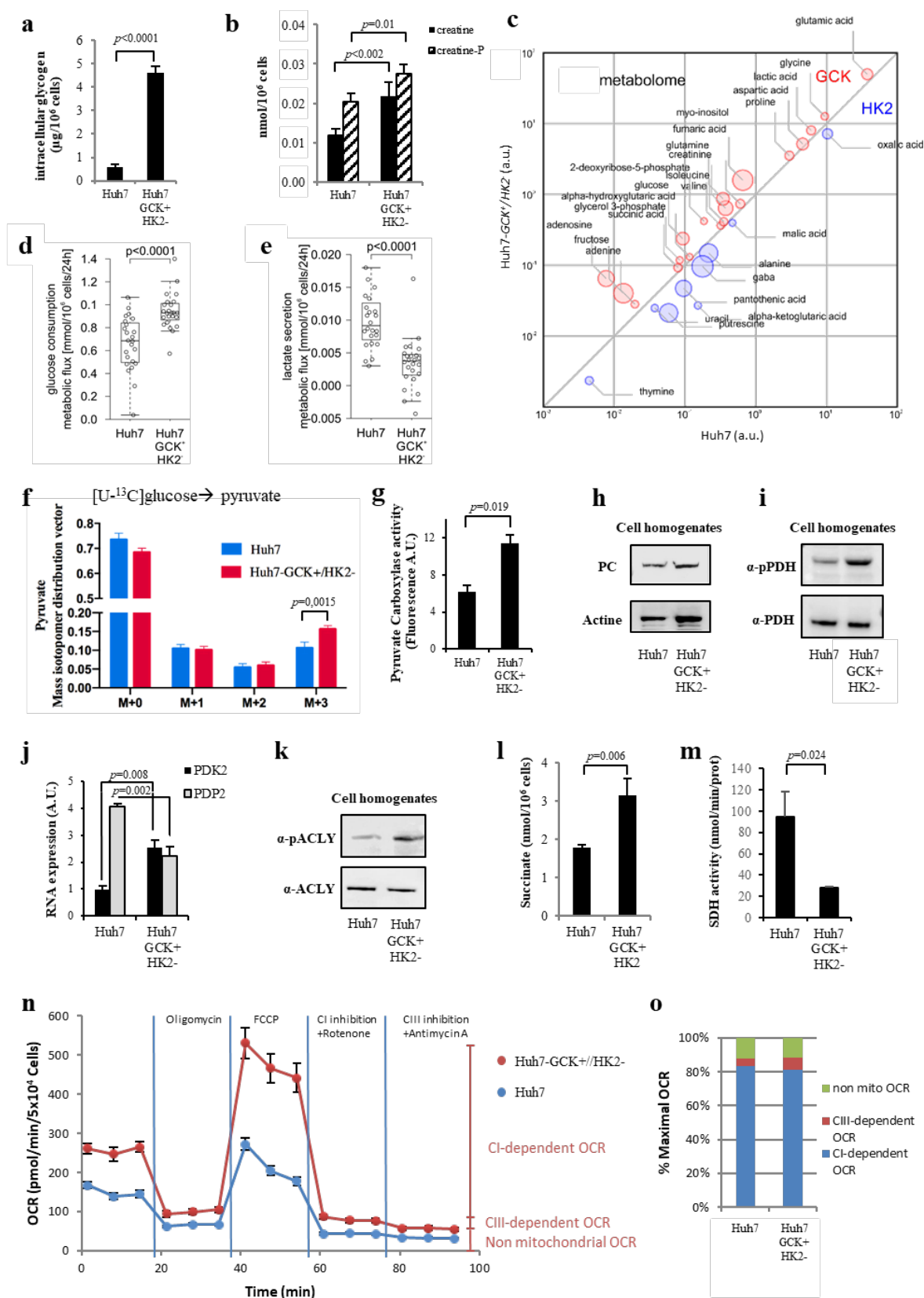
764   **Figure 5. TCA rewiring after hexokinase isoenzyme switch in Huh7 cells**. **a** Glycogen
765   quantification. **b** Creatinine and creatinine-P quantification. **c** This bubble chart compares
766   intracellular metabolomes of Huh7 and Huh7-*GCK+/HK2-* cells. Metabolite pool sizes larger in
767   Huh7 are indicated in blue, whereas the one larger in Huh7-*GCK+/HK2-* are shown in red. The size
768   of bubbles inversely scales with p values between 5.10^{-2} and 1.10^{-17} of differential metabolomics
769   responses. **d, e** Metabolic fluxes for overall glucose consumption (d) and lactate secretion (e) by
770   Huh7 and Huh7-*GCK+/HK2-* cells. Indicated values correspond to differences in glucose or lactate
771   concentrations in extracellular culture medium before and after 24h of culture. **f** Mass isotopomer
772   distribution vector of pyruvate in cells cultured with [U-^{13}C]-glucose. **g** Pyruvate carboxylase (PC)
773   activity determined in cell homogenates. **h** Western-blot analysis of PC expression in Huh7 and
774   Huh7-*GCK+/HK2-* cells. **i**) Western-blot analysis of pyruvate dehydrogenase (PDH) E1-alpha subunit
775   phosphorylation at Ser293. **j** RNAseq quantification of pyruvate dehydrogenase kinase 2 (PDK2)
776   and pyruvate dehydrogenase phosphatase 2 (PDP2)(BH adjusted p value<0.05 from
777   transcriptomic data). **k** Western-blot analysis of ATP-citrate Lyase (ACLY) phosphorylation at
778   Ser455. **l** Succinate quantification in cell homogenates. **m** Succinate dehydrogenase (SDH) activity
779   determined in cell homogenates. **n** Oxygen consumption rate (OCR) in Huh7 and Huh7-*GCK+/HK2-*
780   cells was determined with a Seahorse analyzer before and after the addition of oligomycin
781   (Complex V inhibitor), FCCP (uncoupling agent), rotenone (Complex I inhibitor) and antimycin A
782   (Complex III inhibitor). **o** Non-mitochondrial, complex I-dependent and complex III-dependent
783   maximal OCR were calculated from n. Data correspond to means ± SEM (n≥3).

34

784

a

IFN-I signaling genes

- 20 — More expressed in Huh7-GCK+/HK2-
- 2 — More expressed in Huh7
- Unchanged 69

b

Gene ID	Huh7 (mean normalized counts)	Huh7-GCK+/HK2- (mean normalized counts)	FC (calculated by DESeq2 analysis)
EGR1	178,2	537,5	3,0
GBP2	243,0	816,5	3,3
HLA-A	247,2	608,1	2,5
HLA-B	13,4	29,8	2,2
HLA-H	177,8	579,0	3,3
HSP90AB1	0,0	622,9	10000,0
IFI35	50,2	252,5	5,0
IFI6	21,7	142,8	6,6
IFIH1	34,5	106,1	3,1
IFITM3	180,9	1081,4	6,0
IKBKE	0,3	419,4	1284,3
IRF1	212,9	505,2	2,4
IRF3	38,5	84,4	2,2
IRF9	109,3	388,8	3,6
ISG15	89,9	197,6	2,2
MX1	0,0	28,6	10000,0
OAS1	0,8	157,5	173,5
OAS3	195,1	1095,0	5,6
PSMB8	0,0	13,4	80,0
RNASEL	0,0	4,9	10000,0
ABCE1	6559,7	3037,7	-2,2
TRIM6	663,1	263,9	-2,5

c

ISRE induction (normalized luciferase ratio)

3p-hpRNA: 0, 10, 100, 500 ng/ml; poly(I:C): 0, 10, 100, 1000 ng/ml

p=0.039, p=0.047, p=0.0003

Huh7, Huh7-GCK+/HK2-

d

ISRE induction (normalized luciferase ratio)

0, 3p-hpRNA 100 ng/ml

p=0006, p<0.0001, ns, ns

Huh7, Huh7-HK2+/GCK+, Huh7-GCK+/HK2-, Huh7-GCK+/HK2-Sh

e

IL-6 — pg/ml; p=0.02, p=0.0001

IL-8 — pg/ml; p=0.006, p=0.049

IP-10 — pg/ml; p=0.023, p=0.016

IFN-λ1 — pg/ml; p=0.0026, p=0.048

IFN-λ2/3 — pg/ml; p=0.0008

IFN-β — pg/ml; p<0.0001

3p-hpRNA: 0, 100, 500 ng/ml; poly(I:C): 100, 1000 ng/ml

Huh7, Huh7-GCK+/HK2-

f

% Lysis

E:T Ratio: 0, 3, 30

ns, p=0.018, p=0.011

Huh7, Huh7 GCK+/HK2-

785 **Figure 6. Innate immune response is enhanced in Huh7-GCK⁺/HK2⁻ cells. a** Sector chart from the
786 transcriptomic study showing genes included in the GO-term "Type I-IFN signaling pathway". **b**
787 List of genes significantly up-regulated in purple or down-regulated in green (|FC|>2, BH adjusted
788 *p* value<0.05) in Huh7-*GCK⁺/HK2⁻* compared to Huh7 cells. **c-e** Cells were stimulated or not for 48h
789 with 3p-hpRNA (RIG-I ligand) or poly(I:C) (IFIH1/MDA5 ligand). ISRE-luciferase expression was
790 monitored and normalized to Renilla luciferase (c, d). Cell supernatants were assayed for cytokine
791 concentration by multiplex assays (e). **f** NK cell mediated lysis of Huh7 or Huh7-*GCK⁺/HK2⁻*.
792 Hepatoma cells were seeded 24h before NK cells addition for 4h at effector to target (E:T) ratio of
793 0, 3 or 30. After harvesting, cell lysis was determined by the percentage of PI+ cells on gated
794 hepatocytes. *p* values were obtained from 2-way ANOVA analyses comparing matched cell means
795 with Sidak's correction for multiple comparison, with α=0.05.

796

797

798
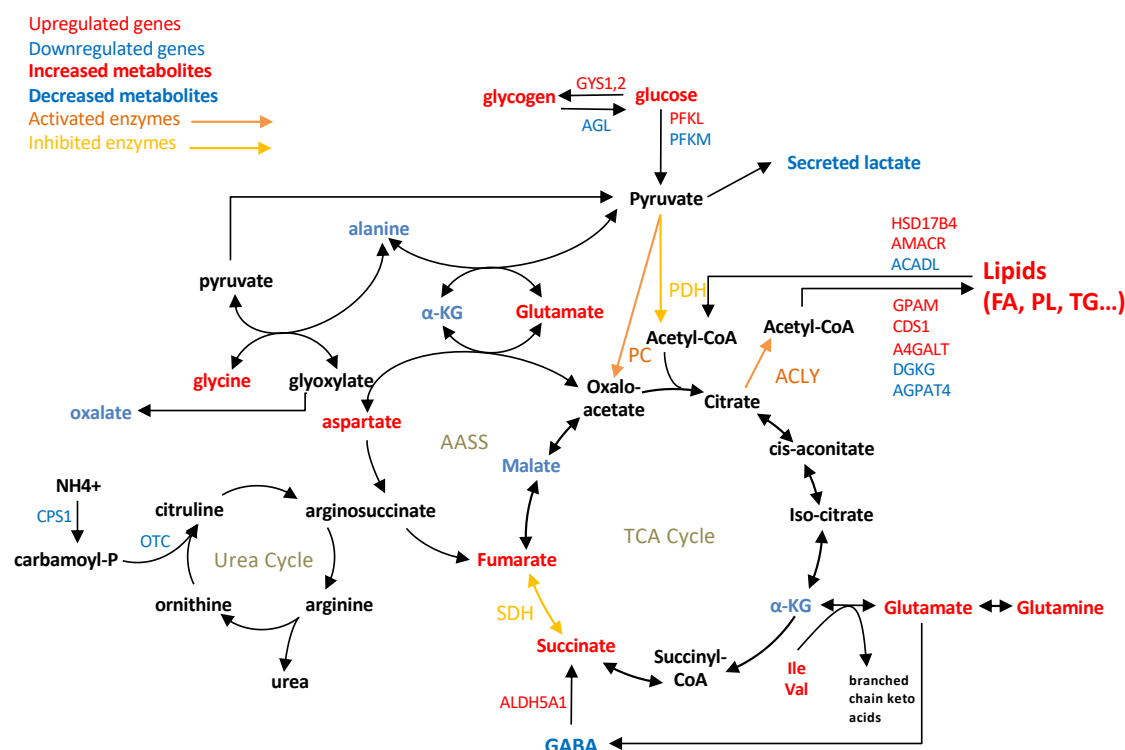
Figure 7. Simplified scheme of central carbon metabolism and connected pathways showing differences between Huh7-$GCK^+/HK2^-$ vs Huh7. Highlighted metabolites, enzymatic activities, and metabolism-associated genes were selected from transcriptomic (Fig. 2e), metabolomic (Fig. 5c) and enzymatic analyses (Fig. 5g-m).

803